Protein Science (1999), *8*:2258–2269. Cambridge University Press. Printed in the USA.

Crystal structure of brain-type creatine kinase at 1.41 Å resolution

MICHAEL EDER,[1,2] UWE SCHLATTNER,[1] ANDREAS BECKER,[2] THEO WALLIMANN,[1] WOLFGANG KABSCH,[2] AND KARIN FRITZ-WOLF[2]

[1]Institute of Cell Biology, Swiss Federal Institute of Technology, ETH Zurich, CH-8093 Zurich, Switzerland
[2]Department of Biophysics, Max-Planck Institute for Medical Research Heidelberg, Jahnstr. 29, D-69120 Heidelberg, Germany

(RECEIVED May 17, 1999; ACCEPTED July 23, 1999)

Abstract

Excitable cells and tissues like muscle or brain show a highly fluctuating consumption of ATP, which is efficiently regenerated from a large pool of phosphocreatine by the enzyme creatine kinase (CK). The enzyme exists in tissue—as well as compartment-specific isoforms. Numerous pathologies are related to the CK system: CK is found to be overexpressed in a wide range of solid tumors, whereas functional impairment of CK leads to a deterioration in energy metabolism, which is phenotypic for many neurodegenerative and age-related diseases. The crystal structure of chicken cytosolic brain-type creatine kinase (BB-CK) has been solved to 1.41 Å resolution by molecular replacement. It represents the most accurately determined structure in the family of guanidino kinases. Except for the N-terminal region (2–12), the structures of both monomers in the biological dimer are very similar and closely resemble those of the other known structures in the family. Specific Ca^{2+}-mediated interactions, found between two dimers in the asymmetric unit, result in structurally independent heterodimers differing in their N-terminal conformation and secondary structure.

The high-resolution structure of BB-CK presented in this work will assist in designing new experiments to reveal the molecular basis of the multiple isoform-specific properties of CK, especially regarding different subcellular locations and functional interactions with other proteins. The rather similar fold shared by all known guanidino kinase structures suggests a model for the transition state complex of BB-CK analogous to the one of arginine kinase (AK). Accordingly, we have modeled a putative conformation of CK in the transition state that requires a rigid body movement of the entire N-terminal domain by rms 4 Å from the structure without substrates.

Keywords: brain-type creatine kinase; cancer; cellular energy metabolism; guanidino kinase; neurodegenerative disorders

Creatine kinase (CK, EC 2.7.3.2), catalyzing the reversible phosphoryl transfer between ATP and creatine (Cr), plays an important role in the buffering and transport of high-energy phosphates via phosphocreatine (PCr) to sites of ATP utilization where the enzyme is associated with ATP-dependent processes, e.g., the contractile apparatus and membrane ion pumps (reviewed in Wallimann et al., 1992). The CK isoform family has been phylogenetically conserved from sea urchin to man (Mühlebach et al., 1994). In mammals, three "cytosolic" dimeric CK isoforms are found: muscle-type MM-CK, ubiquitous brain-type BB-CK homodimers, and MB-CK heterodimers (Eppenberger et al., 1967). In addition, two mitochondrial CK isoforms, existing in dimeric as well as octameric forms, ubiquitous Mi_a- and sarcomeric Mi_b-CK, have been identified and characterized (Schlegel et al., 1988a, 1988b).

The brain-type cytosolic isoform of creatine kinase, BB-CK, is a major enzyme of cellular energy metabolism in nonmuscle cells, found in a variety of tissues, mainly in the brain and in retina, but also in uterus, placenta, kidney, testis, spermatozoa, endothelial cells, and others, where it is mostly co-expressed with Mi_a-CK (reviewed in Wallimann & Hemmer, 1994). Significant fractions of BB-CK are subcellularly associated with ion transport pumps in the brain (Kaldis et al., 1996), kidney (Guerrero et al., 1997), parietal cells of the stomach (Sistermans et al., 1995), gills (Kültz & Somero, 1995), and salt glands (Friedman & Roberts, 1992). The expression of BB-CK is regulated in a tissue-dependent manner (Ritchie et al., 1991) and the subcellular localization of cytosolic CK in developing skeletal muscle is highly isoenzyme-specific (Wallimann et al., 1983).

BB-CK represents the major estrogen-regulated protein in uterus and placenta (Reiss & Kaye, 1981; Payne et al., 1993). The enzyme is stimulated in a sex-specific way by sex steroids (Sömjen et al., 1989) and by Vitamin D (Ch'ng & Ibrahim, 1994).

The CK/PCr system is critically involved in the function of the adult central and peripheral nervous system as well as in embryonic and postnatal brain development (Wallimann & Hemmer, 1994). Furthermore, PCr may serve as a direct energy source for

Reprint requests to: Wolfgang Kabsch, Max-Planck Institute for Medical Research Heidelberg, Department of Biophysics, Jahnstr. 29, D-69120 Heidelberg, Germany; e-mail: kabsch@mpimf-heidelberg.mpg.de.

glutamate uptake into synaptic vesicles (Xu et al., 1996). On the other hand, a deteriorated energy metabolism is a common phenotype for many neurodegenerative disorders of very different genetic etiologies as well as many age-related diseases. For example, BB-CK is dramatically inhibited in Alzheimer's and Pick's disease (Aksenov et al., 1997) and, in addition, an aberrant cytosol-membrane partitioning of BB-CK is seen in Alzheimer's (David et al., 1998). Inactivation of CK, which compromises the cellular energy state, could lead to an increase in the intracellular free calcium, membrane depolarization, and ultimately to cell death by apoptosis.

BB-CK is overexpressed in a wide range of solid tumors and tumor cell lines, e.g., small-cell lung carcinoma, colon and rectal adenocarcinoma, breast and prostate carcinoma, as well as in neuroblastoma (Shatton et al., 1979; Wallimann & Hemmer, 1994). One mechanism leading to BB-CK overexpression is the oncogenic activation linked to adenovirus E1a, since the BB-CK promotor contains a response element for the adenovirus E2E gene product (Kaddurah-Daouk et al., 1990). Furthermore, BB-CK is negatively regulated by the tumor-suppressor activity of p53 (Zhao et al., 1994). It seems as if one function of increased BB-CK levels is to sustain the high energy turnover of these malignant cells, since they often contain high amounts of PCr and are growth-inhibited by cyclocreatine (cCr), whose phosphorylated form is a poor CK substrate and may function as CK inhibitor. Several Cr analogs with cytotoxic effects were described (Bergnes et al., 1996) and have established BB-CK as a promising and novel target for anticancer chemotherapeutic drug design.

The expression of BB-CK from a single gene includes alternative splicing (Wirz et al., 1990), multiple ribosomal initiation (Soldati et al., 1990), and various post-translational modifications (Quest et al., 1990). For the chicken B-CK gene, an alternative splicing mechanism produces two slightly different B-CK subforms: B_a (acidic)- and B_b (basic)-CK. Modifications at the protein level include autophosphorylation (Hemmer et al., 1995) and phosphorylation, most likely mediated by protein kinase C (Chida et al., 1990), the latter leading to a reduction of the K_m for PCr (Quest et al., 1990). All these mechanisms give rise to the notorious microheterogeneity of BB-CK seen on two-dimensional gels, which prevents the formation of high quality crystals from protein isolated from tissues.

So far, crystal structures of members of the guanidino kinase family have been determined for the octameric chicken Mi_b-CK at 3 Å resolution (Fritz-Wolf et al., 1996) by isomorphous replacement, rabbit MM-CK (Rao et al., 1998), and horseshoe crab arginine kinase in the transition state (Zhou et al., 1998) at 2.35 and 1.86 Å resolution, respectively.

In this study, we report the structure of BB-CK at atomic resolution obtained from high quality crystals of the chicken isoform recombinantly expressed in *Escherichia coli*. Knowledge of this structure is expected to help in understanding isoform specific functions and subcellular targeting of BB-CK as well as its possible role in many pathologies.

Results and discussion

Structure determination and model accuracy

The observed amino acid sequence identity between chicken mitochondrial Mi_b-CK and cytosolic brain-type BB-CK is 60% (Mühlebach et al., 1994), which suggests a similar three-dimensional structure for both isoforms. Consequently, the structure was solved by molecular replacement using the coordinates of the chicken mitochondrial isoform of creatine kinase determined at 3.0 Å resolution (Fritz-Wolf et al., 1996).

The refined model fits the observed data to 1.41 Å resolution with a free *R*-factor of 18.8% (R_{cryst} = 13.4%, including anisotropic *B*-factor refinement). The coordinate error of the model, as deduced from a Luzatti plot (Luzatti, 1952), is 0.1 Å. Relevant refinement and model statistics are shown in Table 1.

The crystallographic asymmetric unit contains two homodimers of BB-CK. The final model includes all residues of the four monomers, one Ca^{2+} ion, 6 acetate and 1,467 water molecules. Alternative conformations were assigned for 15 residues. Electron density was absent for a highly flexible loop (residues 321–331). Weak density remains for the second flexible loop (residues 66–70) and for some side chains at the surface of the protein, whereas both N- and C-termini are clearly defined.

Overall structure

Biologically active BB-CK dimers with a molecular mass of 2 × 43 kD and overall dimensions of ~92 × 42 × 65 Å display an elongated "banana-like" shape (Fig. 1), as noted earlier on electron micrographs of dimeric Mi-CK (Schlegel et al., 1988a). The two dimers (named A:B and C:D, respectively) in the asymmetric unit are held together along the crystal *c*-axis by Ca^{2+} ions, which explains the essential role of these ions for crystal formation (Fig. 2A). Each ion is octahedrally coordinated by a carbonyl oxygen of Lys41 and Asp44 side-chain oxygens of monomer A and monomer D (Fig. 2B,C). As we unambiguously observe a different chain fold in the electron density map, these interactions apparently give rise to two clearly distinguishable monomers in the biological homodimer. It is unknown whether this unexpected Ca^{2+}-mediated interaction seen between BB-CK dimers is of significance in vivo, where it could support an attachment of BB-CK dimers to subcellular components (e.g., ion pumps).

The fold of the monomer (B-CK) is very similar to that of the mitochondrial isoform and to the recently solved cytosolic muscle-

Table 1. *Summary of the final model*

No. of reflections used in refinement	282,461
No. of reflections used for R_{free}	14,886
No. of parameters refined	122,049
Resolution range	6.0–1.41
R_{cryst} (%)	13.4
R_{free} (%)[a]	18.8
No. of atoms in the model	
Protein (nonhydrogen)	12,067
Hydrogen	11,644
Water	1,467
Ions	25
No. of residues with disorder	15
B-factor model	Anisotropic, restrained individual
rms deviation	
Bonds (Å)	0.011
Angle distances (Å)	0.029

[a] *R*-factor calculated for 5% of randomly chosen reflections that were excluded from the refinement.

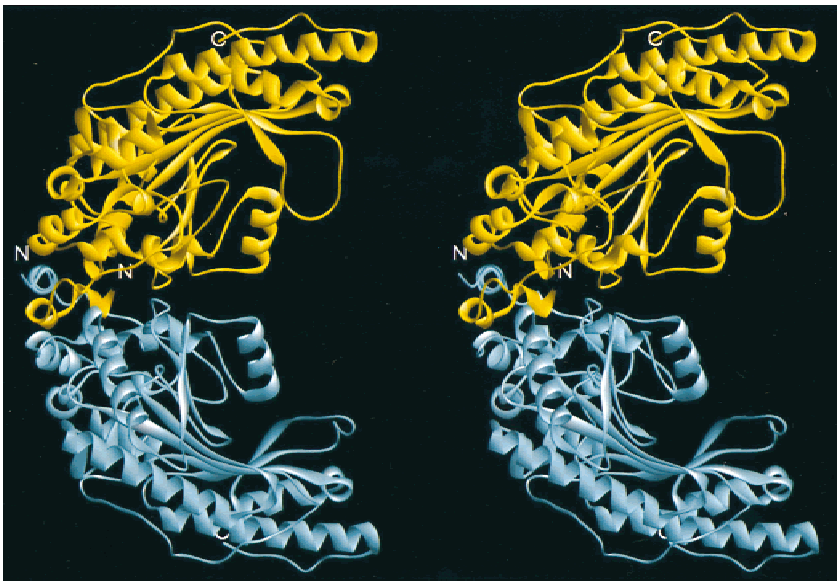

Fig. 1. Stereo view of a "banana-shaped" biologically active dimer of chicken BB-CK in a ribbon representation. Monomer A and B are shown in cyan and yellow, respectively. Note the different topology of the N-termini located between the monomers. This figure was prepared with WebLabViewer Lite V.3.1 (MSI Inc., San Diego, California).

type MM-CK (Rao et al., 1998), as well as to arginine kinase (Zhou et al., 1998). As shown in Figure 3, B-CK consists of a small N-terminal domain comprising residues 2–100 and a larger C-terminal domain (residues 125–381) connected by a long linker region (101–124). The large domain contains an eight-stranded antiparallel β-sheet flanked by seven α-helices, which resembles the C-terminal domain of glutamine synthetase (Liaw et al., 1994; Kabsch & Fritz-Wolf, 1997). The N-terminal domain is made up of seven α-helices (monomer A and D) or of two 3_{10}-helices and six α-helices (monomer B and C). Residues 6–13 of monomer A and D form a regular α-helix, whereas residues 3–7 and 9–13 of monomer B and C form two 3_{10}-helices. Moreover, the N-termini of monomer A and D are located at the surface of the dimer, while the first eight residues of monomer B and C protrude into the contact region between the two monomers (Figs. 1, 2B). They have a markedly lower *B*-factor (8–15 Å^2) compared to the corresponding stretches of monomer A and D, which can be explained by numerous strong interactions with residues of both monomers and water molecules located at the interface (see below). A section of the electron density map from this region is shown in Figure 4. The finding of two remarkably different N-terminal conformations in a homodimeric protein seems to be noteworthy and differs from the structure of the previously solved chicken Mi_b-CK, where the two monomers building the biologically active dimer are identical. Whether this is a feature unique to BB-CK or a general property of cytosolic creatine kinases cannot be answered at the moment, since in the structure of rabbit MM-CK residues 2–7 were not defined by electron density (Rao et al., 1998).

Additional structural differences between the monomers are found for residues at the surface and for flexible loop regions of the enzyme. Otherwise, structural differences between the monomers are rare, especially in the highly conserved "common core" of all guanidino kinases. Pairwise superposition of the four crystallographically independent monomers, excluding residues 2–8 and the flexible loop residues 322–330, results in rms deviations of only 0.3–0.5 Å for C_α atoms and 0.7–0.9 Å for all atoms.

The monomer–monomer interface

All CK isoforms are known to form extremely stable dimers, which can be dissociated only under drastic conditions along with partial unfolding of the monomer (Gross et al., 1995). For BB-CK, 18 hydrogen bonded interactions and 4 salt bridges are found between the monomers. Additionally, 20 hydrogen bond interactions mediated by a water molecule were identified, which contribute to the observed remarkable stability of creatine kinase dimers. The importance of water molecules for oligomerization has been emphasized in a survey on homodimeric protein interfaces (Larsen et al., 1998). Creatine kinase seems to be yet another example where direct protein–protein interactions alone cannot explain the experimentally observed high oligomer stability.

The active site

Creatine kinase contains several conserved arginines in the active site (Arg96, 130, 132, 135, 236, 292, and 320). By comparison with the structures of chicken Mi_b-CK with bound Na-ATP (Fritz-Wolf et al., 1996) and the transition state structure of horseshoe crab arginine kinase (Zhou et al., 1998), arginines 130, 132, 236, 292, and 320 of B-CK are expected to interact with the phosphate groups of the adenine nucleotide. In the current structure, neither substrates nor phosphate ions were present, resulting in higher temperature factors and some disorder for the respective arginines. Surprisingly, none of the negatively charged buffer acetate ions, although present at 0.8 M concentration in the crystallization buffer, could be located in the proximity of these arginines in the electron density map.

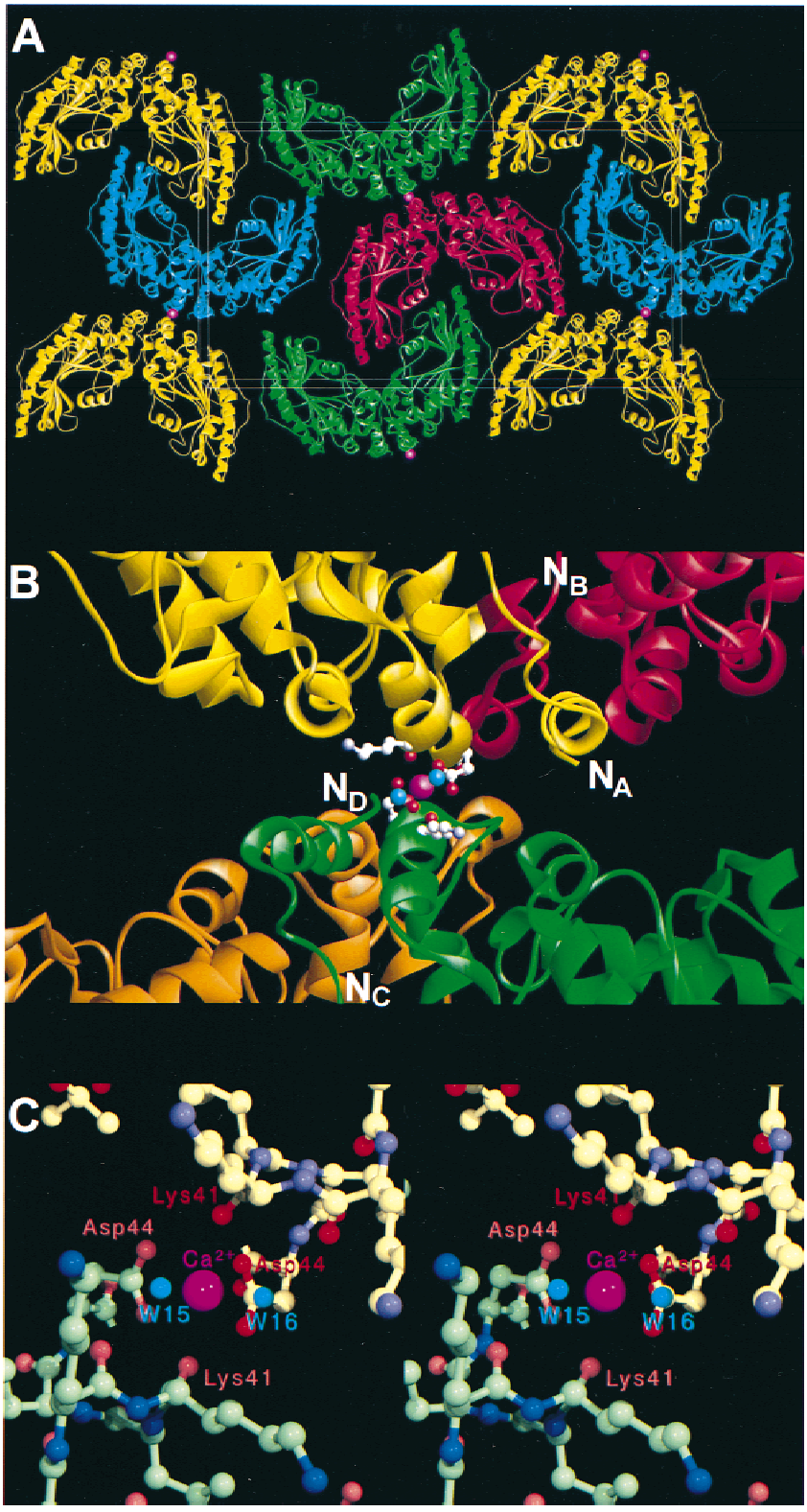

Fig. 2. Ca^{2+}-mediated packing of BB-CK dimers. **A:** Crystal packing of BB-CK dimers in the unit cell. The calcium ion shown in magenta is located between two dimers of BB-CK. **B:** Magnification of **A**, which includes ball-and-stick representations of Lys41 and Asp44 in monomers A and D involved in Ca^{2+} coordination. The N-termini of the four monomers A–D are marked for clarity. Panels **A** and **B** were produced using WebLabViewer Lite V.3.1 (MSI Inc.). **C:** Stereo view of the octahedral coordination sphere around the Ca^{2+} ion. Carbon atoms of monomer A and D are color-shaded in yellow and green, respectively. All other atoms are shown in standard colors. The six ligands of the Ca^{2+} ion comprise carbonyl oxygens of Lys41 and side-chain oxygens of Asp44 of monomers A and D, as well as two water molecules (shown in cyan). Panel **C** was prepared with Swiss-PDBViewer V. 3.1 (N. Guex, Glaxo Wellcome Experimental Research) and subsequent rendering with POVRay V. 3.1 (http://www.povray.org).

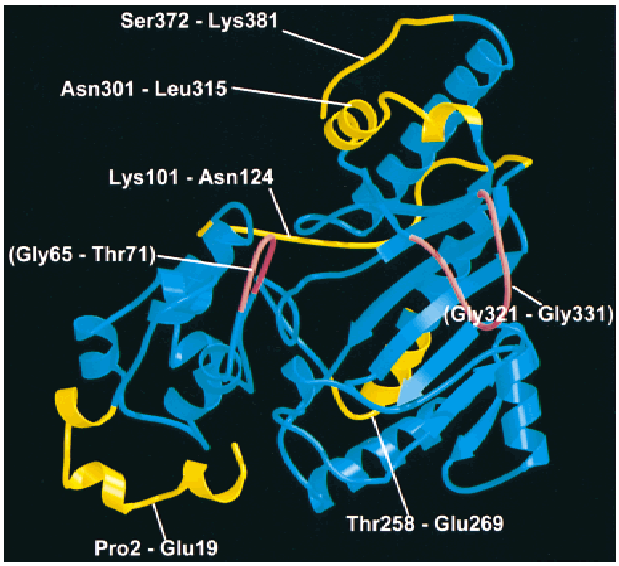

Fig. 3. Ribbon representation of a B-CK monomer (monomer B). The conserved "common core" of all CK isoenzymes is shown in cyan, isoenzyme-specific sequences are coded in yellow, together with the B-CK numbering of these residues. Two flexible loops conserved in all CKs and known to be important for catalysis are depicted in light red with the respective residue numbers in brackets. This figure was prepared with MOLSCRIPT (Kraulis, 1991) and Raster3D (Merritt & Bacon, 1997).

The strictly conserved residues Glu231, Glu232, and Asp233 form a compact negatively charged cluster, which is absolutely essential for catalysis (M. Eder, in prep.). The unusual backbone conformation of Glu231, which is only generously allowed as defined by the program Procheck (Laskowski et al., 1993), is fully confirmed by unambiguous electron density. Comparison with the transition state structure of arginine kinase reveals that Glu231 could participate in the coordination of the essential Mg^{2+} ion via two bridging water molecules, whereas Glu232 is most likely involved in positioning the guanidino group of creatine. Asp233 forms a hydrogen bond with the backbone amide of Thr282 thus fixing the shape and stereochemistry of the active site. The loop 280–285 contains the highly reactive "essential" Cys283, the function of which has been heavily debated (Beuchter et al., 1992; Hou & Vollmer, 1994; Stroud, 1996).

However, a careful kinetic analysis of several site-directed mutants of Cys283 clearly showed that this residue is not directly involved in catalysis but plays a role in substrate binding synergism (Furter et al., 1993). The γ-sulfhydryl group of Cys283 is in hydrogen bond distance (3.0 Å) to Ser285 and does not change its relative position when compared to the transition state structure of AK. In the AK structure, the distance of Cys271 to the corresponding conservatively replaced Thr273 (AK numbering) was found to be identical. Interestingly, Thr273 is connected via one water molecule to one oxygen of the nitrate group, which, in the transition state analog complex, mimics the planar γ-phosphoryl group of ATP that is transferred to Cr. Mutagenesis experiments with human Mi_b-CK replacing Ser285 to alanine/aspartate corroborate the importance of this residue for catalysis (M. Eder, in prep.).

The presence of a single cis-proline at position 212, as already postulated for Mi_b-CK, can be confirmed unequivocally in the present high-resolution structure. This cis-proline is conserved throughout all guanidino kinases including the recently solved arginine kinase. It is located between β-strand 3 (216–220) and a loop (residues 204–211), which covers part of the active site cleft. Mutation of this proline leads to a reduction of enzyme activity and a pH shift in the pH optimum of the CK reaction by 1.3 pH units toward acidic pH (Forstner et al., 1998a).

Flexible regions

In the current structure of B-CK, three main regions exhibiting conformational flexibility and high average *B*-factors are present. Residues 66–70 form a flexible loop (Fig. 3) characterized by high temperature factors and solvent exposure of hydrophobic residues, as it was already seen in the chicken Mi_b-CK structure. Only weak electron density was found in particular for the side chains of His66 and Phe68. This loop was postulated to act as a lid for the active site thereby excluding water from catalysis (Fritz-Wolf et al., 1996). Mutation of His61 in Mi_b-CK (corresponding to His66 in BB-CK) severely hampers enzyme activity (Forstner et al., 1997) corroborating the proximity of this loop to the active site in the working enzyme. Guanidino kinases differ significantly in the length of this loop depending on the size of the guanidino substrate (Suzuki et al., 1997). AK has a shortened loop to accommodate the relative bulky arginine, whereas CK uses four additional residues to effectively cover the active site containing the smaller creatine molecule. In the AK structure, the loop residues have low *B*-factors as expected for a "closed" conformation with bound substrates. Recently, cross-linking experiments with rabbit MM-CK and the creatine "analog" N-dibenzylphospho-N′-(4-benzoyl)-benzylguanidine (BzPG) identified this region to be involved in creatine binding (Min et al., 1998). The second flexible loop of B-CK consists of residues 321–331, for which no significant density is found in our structure (Fig. 3). Some of these residues exhibit unusual backbone conformations as judged from a Ramachandran plot. In some cases these Ramachandran violations could not be resolved due to crystal packing interactions with symmetry related monomers. The final position of this loop for catalysis can only be determined in the transition state as seen for AK (Zhou et al., 1998). Again, the corresponding AK loop 310-320 is well defined with *B*-factors even less than the average for the whole structure. The third flexible region includes α-helix 9 (181–190), which is located at the surface of the molecule. Superposition of BB-CK with the "closed" AK-structure reveals striking differences in this area. The AK region corresponding to B-CK residues 172–214 (including α-helix 9) has moved substantially toward the active site (see below).

By analogy, we expect the described flexible regions in the BB-CK structure to undergo large conformational changes during catalysis.

Comparison of CK isoforms

With both the structures of chicken Mi_b-CK and rabbit MM-CK at hand, one can now compare the crystal structures of three different isoforms of CK. Isoenzyme specific sequence stretches of the B-CK monomer are indicated in Figure 3. These include the N-terminus (residues 2–19), the linker region between the two domains (101–124), part of α-helix 11 (258–269), α-helices 12 and 13 (301–315), and the C-terminus (372–381). Except for the N-terminal region, where CK isoenzymes diverge most significantly in their amino acid sequences, the other isoenzyme specific stretches display a conserved backbone structure. As expected, isoenzyme specific

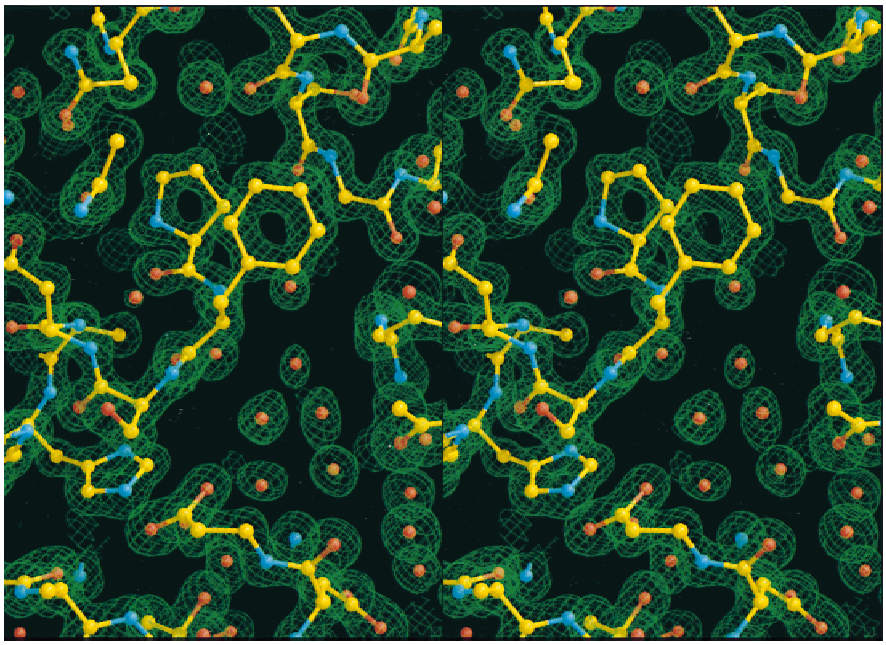

Fig. 4. Stereo view of the final σ_A-weighted $2F_o - F_c$ map at 1.41 Å and contoured at 1.6σ, showing the quality of the final BB-CK model. The view is centered at the monomer–monomer interface showing the N-terminus of monomer B around Phe3. Several water molecules drawn as red spheres can be located at the interface. The figure was prepared using XtalView 3.2+ (McRee, 1992) and Raster3D (Merritt & Bacon, 1997).

residues are located in solvent accessible regions at the surface of the enzyme. Obviously, most of the differential properties of CK isoenzymes have to be explained by differences in their primary sequence, which result mainly in electrostatic potential changes at the surface of the enzyme.

BB-CK and Mi$_b$-CK

Isoform specific structural differences comprise the overall shape of the dimers, the N-terminal region (residue 2–20 for BB-CK and 1–15 for Mi$_b$-CK), the linker region (101–124 for BB-CK and 96–119 for Mi$_b$-CK), and the C-terminal end.

Superposition of the dimers of these two isoenzymes resulted in an overall rms difference of 1.24 Å (for 716 pairs of C_α-atoms). This calculation does not include residues 2–11 (N-terminus), 116, 119, and 324–329, which are too different to be included in the comparisons. The largest differences in the superimposed structures are found for residues 300–306 and 363–380, because the curvature of the "banana-shaped" dimers appears to be larger for BB-CK when compared to Mi$_b$-CK. In fact, if one superimposes only a single monomer of each structure, the RMS difference is substantially lower (0.72 Å for 358 C_α pairs). These differences corroborate the finding of CK being a flexible hinge-bending enzyme with relatively large domain movements during catalysis, as indicated earlier from immuno-enzymological experiments (Samuels, 1961), fluorescence (Grossman, 1990), and infrared spectroscopy (Raimbault et al., 1996), as well as X-ray scattering studies in solution (Forstner et al., 1998). The observed difference in the overall structure could well be a consequence of weak packing interactions in the crystal.

The largest differences between the two structures can be found in their N-terminal region. Additionally, the mitochondrial isoforms lack the first four residues at the N-terminus. In the case of Mi$_b$-CK, mutagenesis studies demonstrated the importance of the N-terminus for octamer stability (Kaldis et al., 1994). Deletion of the N-terminal heptapeptide and simultaneous mutation of the dimer/dimer interface Trp264 significantly reduces octamer formation of Mi$_b$-CK. The N-terminus of chicken Mi$_b$-CK protrudes into the ~20 Å wide central channel of the octamer, probably fulfilling the role of interacting with ordered water molecules located in this channel. This assumption is supported by the fact that in all mitochondrial isoforms residues 5–7 carry a positive net charge. For the cytosolic CKs, which exclusively form dimers, the function of their N-termini must be different. The N-terminus of BB-CK is closer to the dimer interface or even buried between the interface, thus yielding additional interactions with residues of the same or the contacting monomer. Moreover, the surface area buried by forming the BB-CK dimer (1,851 Å^2) significantly exceeds the area found for Mi$_b$-CK dimers (1,337 Å^2), as calculated by DSSP (Kabsch & Sander, 1983). It is likely that the additional interactions and the larger contact surface found in BB-CK lead to increased dimer stability compared to the mitochondrial isoforms. However, experimental evidence for this hypothesis is lacking, since none of the numerous unfolding and stability studies done so far have included BB-CK for comparison.

The linker region of the cytosolic isoforms between N- and C-domain (residues 101–124) shares only little sequence homology with the mitochondrial isoenzymes. This observation is consistent with the model proposing this region as one of the possible membrane binding motifs specific for the mitochondrial CK isoforms (Schlattner et al., 1998). Indeed, this linker region is located at the surface of the octamer with the side chains pointing toward the fourfold top or bottom faces of Mi-CK. In the B-CK structure, the course of the backbone does not differ substantially with only the side chains having different sequence and conformation.

The second putative membrane-binding region of Mi-CKs resides at the very C-terminal end of the molecule. Compared to the cytosolic CKs, Mi-CKs have three to four additional residues (depending on the isoform) carrying two positive charges, which could interact with the negatively charged head groups of cardiolipin in the mitochondrial membranes. In the B-CK structure, an additional short 3_{10}-helix is found for residues 373–375. A specific function for the C-terminus of the cytosolic isoforms has not yet been found, although it is known that the latter also can bind to phospholipid membranes (Rojo et al., 1991).

BB-CK and MM-CK

The two cytosolic isoforms share 77–82% amino acid sequence identity (Mühlebach et al., 1994), pointing to high conformity of their three-dimensional structures. Indeed, no significant divergence in the overall fold is seen. Rms deviations for superimposed BB- and MM-CK dimers are 1.42 Å for 724 C_α pairs and, if only the monomers are considered, 1.12 Å for 362 C_α pairs.

A small proportion (5–10%) of MM-CK is specifically bound to the myofibrillar M-band and is functionally coupled to the myofibrillar actin-activated Mg^{2+}-ATPase as an efficient ATP regenerator (Ventura-Clapier et al., 1994). Additionally, several authors have proposed an important function of MM-CK for the structural integrity of the myosin filament lattice. In situ diffusion assays with fluorescently labeled MM-CK and genetically engineered M/B-CK hybrids have identified the N-terminal part of MM-CK to be responsible for the observed differential binding pattern (Stolz & Wallimann, 1998). Very recent data indicate that a mutant BB-CK with only two residues in this region changed to their muscle-type counterparts exhibits the same binding properties to the M-Band as native MM-CK (T. Hornemann, unpubl. data). Since the backbone conformation in this region is nearly identical for both enzymes, the changes in the charge distribution introduced by this mutation obviously plays the main role for the observed differential binding specificity of these two isoenzymes.

Modeling the transition state conformation of BB-CK

A stable dead-end transition state analog complex (TSAC; Milner-White & Watts, 1971) is induced by binding of nitrate (which mimics the transferred phosphoryl group), MgADP and creatine to the active site of CK, leading to a large conformational change of the enzyme (see above) and a dissociation of Mi-CK octamers into dimers (Marcillat et al., 1987; Schlegel et al., 1988b). In the case of arginine kinase (AK), a similar transition state analog complex can be formed with arginine instead of creatine.

The structure of such a complex has recently been solved (Zhou et al., 1998) and allows the generation of a putative transition state conformation of BB-CK by analogy. Both enzymes share a similar subunit topology, although AK is functional as a monomer and shares a much lower overall amino acid sequence identity of ~40%. The sequence identity between active site residues is exceptionally high, which suggests a common catalytic mechanism for all guanidino kinases. The main differences in the structure of the two enzymes occur in the first 25 residues at the N-terminus, in the linker region between the two subdomains (101–124), in the region containing residues 263–270 (with an insertion of five extra residues in CKs) as well as at the C-terminal end. The residues mentioned are known to be exclusively involved in CK-specific structural functions, such as dimer and octamer formation or subcellular localization. Superposition of the "open" B-CK structure with the "closed" AK-structure is shown in Figure 5A. The antiparallel β-sheet forming the back of the active site was used as a reference point for the structural alignment, because they are not expected to be involved in domain movements during catalysis. However, the entire N-terminal domain did not fit at all if the enzymes were superimposed as a rigid body. This is also reflected in a large rms deviation, when structurally equivalent elements of this domain are aligned (residues 27–62 and 74–101 of BB-CK, RMSD 4.81 Å for 64 C_α atom pairs). The second region with poor superposition results comprises residues 176–216. Therefore, we decided to model the putative "closed" conformation by separating a monomer of B-CK into four domains to find individual rotations/translations. Superposition of the entire N-terminal domain (residues 2–99) with the corresponding AK domain leads to substantial movements of BB-CK atoms, which are as large as 6 Å for the flexible loop 66–70, when compared to the initial model (Fig. 5B). The fit obtained by this simple method is excellent and reduces the rms deviation from 4.81 to 0.76 Å (for 64 C_α atom pairs, as above). Obviously, the observed large movement of the N-terminal domain can be explained by a single "rigid body" rotation toward the active site. A good candidate for the pivot point of this hinge bending is Gly99. The second part of CK transformed individually (residues 138–217) does not fit as well as the N-terminal domain, although the fit to the corresponding part of AK is improved, when compared to the initial rigid body approach. This may be due to differences in the course of the peptide chain with one extra insertion for AK in a linker region between helix 6 and 7, or to apparent movements of single helices (e.g., α-helix 9, 181–189), which cannot be explained with the modeling approach chosen. Additionally, the flexible loop 321–331 was modeled onto the corresponding AK loop, so that the side chain of Asp326 is in the proximity of the creatine guanidino group as seen in the AK structure.

The improvement in the overall fit obtained by this method endorses the modeled structure to be consistent with a putative transition state. However, the final answer for the transition state conformation of CK at atomic resolution can only be reached by an X-ray structure including the transition state analog complex compounds. It would be too speculative at the moment to discuss possible "switches" involved in initiating this rather large domain movement. Moreover, we only modeled a monomer of CK into the closed conformation, thus neglecting the observed cooperativity between monomers. Whether this cooperativity is accomplished by a "flip-flop" mechanism with only one active site at a time being involved in the phosphoryl transfer, or by specific interactions that allow both catalytic sites to be active simultaneously, is still unclear and needs further investigations. We suggest this model to be a starting point for initiating new experimental approaches to finally reveal the detailed catalytic mechanism of CK at an atomic level.

Materials and methods

Protein expression and purification

cDNA of mature chicken cytosolic brain-type creatine kinase (b subtype (B_b-CK), EMBL access No. X03509, Hossle et al., 1986) was cloned into a pET-3b derived expression vector (plasmid pT23; Stolz & Wallimann, 1998) and transformed into *E. coli* strain BL21(DE3)pLysS using standard procedures. Chicken BB-CK was subsequently overexpressed after induction with IPTG and cells were harvested about 5 h after induction. Protein was purified according

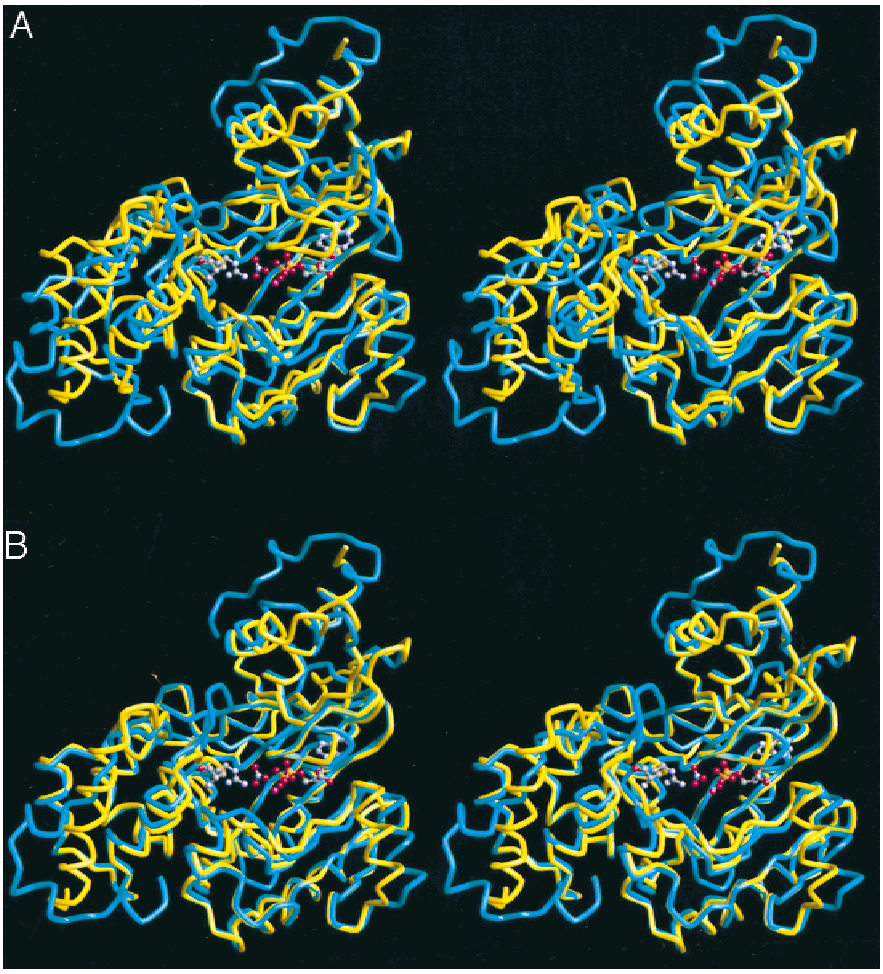

Fig. 5. Superposition of a B-CK monomer with the transition state structure of arginine kinase (AK, Protein Data Bank accession code 1bg0, Zhou et al., 1998). A stereo view of the backbone traces of B-CK and AK is shown in cyan and yellow, respectively. The transition state analog complex components (MgADP, NO_3^-, and arginine), marking the active site of AK, are depicted in a ball-and-stick representation using standard atom colors. **A:** Rigid body superposition of both enzymes using the antiparallel β-sheet as a reference point for the structural alignment (see text). **B:** Modeling of a putative transition state structure of B-CK by superposition of individual domains with AK. B-CK was divided into four domains and aligned individually (see text). This figure was prepared with WebLab-Viewer Lite V.3.1 (MSI Inc.).

to the protocol of Furter et al. (1992) in a slightly modified version (M. Stolz & M. Eder, unpubl. data) as follows. Briefly, the cells were lysed by sonication in 50 mM Tris-HCl, pH 8, containing 10% sucrose. The supernatant was adjusted to pH 5.8 and loaded onto a Blue Sepharose column (Pharmacia, Dübendorf, Switzerland), previously equilibrated with 50 mM NaP_i, pH 5.8. After washing, BB-CK was eluted with NaP_i-buffer at pH 8.3 containing 5 mM MgATP. The sample was concentrated, dialyzed against 25 mM Tris/HCl (pH 8.5), and subsequently purified on a POROS HQ column connected to a high-performance liquid chromatography system (BioCAD, Perkin-Elmer, Rotkreuz, Switzerland) using a NaCl gradient from 0–400 mM. BB-CK eluted at ~150 mM NaCl and was essentially pure (>95%). This protocol yielded ~50 mg purified BB-CK per liter of culture. For crystallization trials, the protein was loaded onto a preparative Sephacryl S300-16/60 column to eliminate remaining impurities. After the final step, BB-CK was >99% pure as judged by SDS-PAGE (not shown).

Due to the expression system used, recombinantly expressed BB-CK lacks the N-terminal methionine, which is encoded by the gene of cytosolic creatine kinases. Although this N-terminal methionine is cleaved off after synthesis in vivo, our amino acids numbering starts with residue 2 to be consistent with the sequence numbering deduced from the gene and used in the literature.

Enzymatic activity of purified BB-CK as well as of redissolved BB-CK crystals were determined using a photometric assay. The production of ATP (reverse reaction) was coupled by hexokinase (300 U/mL) and glucose-6-phosphate dehydrogenase (150 U/mL) to NADPH production, using 2 mM ADP, 5 mM $MgCl_2$, 20 mM PCr, 40 mM D-glucose, and 1 mM NADP in 0.1 M triethanolamine buffer pH 7.

Recombinant BB-CK used in crystallization setups exhibited a specific activity of 240 U/mg protein in the reverse reaction (ATP production).

Crystallization

For crystallization, purified chicken BB-CK was transferred into a new buffer system (20 mM Na-cacodylate, 2 mM DTT, pH 6.5) by

a fast desalting Sephadex G25 M column (Pharmacia PD-10) and concentrated to 10–15 mg/mL by ultrafiltration (Centricon 30, Grace, Beverly, Massachusetts). Initial crystallization setups were prepared by the sitting drop method using the Crystal Screen I–Kit of Hampton Research (Laguna Hills, California) at 22 °C. Small and heavily twinned crystals were obtained at 0.2 M Ca-acetate, 18% PEG 8000, 0.1 M Na-cacodylate, pH 6.5, and 10 mg/mL protein. Subsequent refinement of the crystallization conditions and macroseeding yielded large single crystals suitable for X-ray analysis. Optimal sitting drop growth conditions for BB-CK crystals were as follows: $T = 20$ °C; 8 mg/mL protein in 25 mM MES, 3 mM DTT, 1 mM NaN_3, pH 6.5; reservoir concentration: 0.4 M $Ca(OAc)_2$, 15% PEG 8000, 0.1 M MES, pH 6.5; equal volumes (5 + 5 μL). Macroseeding with small crystals was performed 24 h after setup and yielded rodshaped crystals (~0.5 × 0.3 × 0.2 mm in size) after 5–7 days. Cryoprotection was achieved by soaking the crystals for 1 h with PEG 8000 concentrations raised to 25%. In addition, the concentration of DTT was also increased to 10 mM to restore a fully active enzyme and to prevent any cysteine modifications. For data collection, crystals were picked up with cryo loops (Hampton, Laguna Hills, California, 0.5–0.7 mm loop diameter) and flash cooled by plunging into liquid nitrogen.

Data collection

Diffraction data were recorded by the rotation method. As summarized in Table 2, two native data sets were collected: For initial structure analysis, a low resolution dataset (BBCK-1) was collected from seven crystals at 4 °C in the laboratory (X-rays: CuK_α, focused by Franks double-mirror optics; generator: GX-18, Elliot/Enraf-Nonius, Delft, operated at 35 kV/50 mA; detector: X100, Siemens/Nicolet, Madison, Wisconsin; crystal to detector distance: 13 cm; rotation/image: 0.0417° or 0.0833°). The high resolution dataset (BBCK-2) was obtained from a single crystal at 100 K using synchrotron radiation at the EMBL outstation (DESY Hamburg, Beamline BW7B) (λ = 0.8435 Å; detector: MAR345 imaging plate (MAR Research, Hamburg, Germany); $\Delta\phi = 0.3°$ rotation/image, F = 250 mm crystal to detector distance for the high dose and $\Delta\phi = 1.2°$, F = 340 mm for the low dose pass).

Integrated intensities were extracted from the rotation images by the program package XDS (Kabsch, 1988), which includes routines for scaling data from several crystals as well as for space group determination from the observed diffraction pattern (Kabsch, 1993). BB-CK crystals belong to space group P 2_1 and diffract up to ~1.4 Å. The crystals contain two dimers in the asymmetric unit, resulting in a Matthews coefficient V_M of 2.4 and a calculated solvent content of 48%.

Model building and refinement

An initial structure was found by molecular replacement (Rossmann, 1972) based on dataset BBCK-1 and the coordinates of chicken Mi_b-CK (PDB entry 1crk, Fritz-Wolf et al., 1996), which displays about 60% sequence identity with BB-CK (Mühlebach et al., 1994). Rotation function analysis (programs by W. Kabsch, unpubl.) with a dimer of Mi_b-CK resulted in four peaks of similar height as expected for two dimers of BB-CK in the asymmetric unit. Translation function search by the program AMoRe (Navaza, 1994) with data from 10–3.6 Å revealed the packing of the model in the unit cell.

In subsequent refinement steps, 10% of the reflections were set aside for calculation of the free R-factor (Brünger, 1992a). The initial free R-factor of the model dropped from 44.2 to 40.2% after rigid body minimization (X-PLOR 3.851, Brünger, 1992b). Posi-

Table 2. *Data collection statistics*

Dataset BBCK-1								
λ (Å) = 1.5418	T = 277 K	Sspacegroup $P2_1$		Unit cell: a = 48.61, b = 179.62, c = 95.44, β = 95.59				
Shell (Å)	Overall	∞–6.0	6.0–4.0	4.0–3.0	3.0–2.5			
Unique reflections	52,558	4,083	9,683	17,939	20,853			
Completeness (%)	93.5	99.2	99.9	95.6	88.3			
$\langle I/\sigma \rangle$	10.2	32.7	20.3	8.9	2.2			
Mean redundancy	4.9	12.7	8.6	4.5	1.9			
R_{meas} (%) [a]	11.3	7.6	10.9	14.3	25.5			
$R_{mrgd\text{-}F}$ (%)	9.4	3.3	5.9	9.7	17.9			
Dataset BBCK-2								
λ (Å) = 0.8345	T = 100 K	Spacegroup $P2_1$		Unit cell: a = 48.43, b = 175.99, c = 95.40, β = 95.85				
Shell (Å)	Overall	∞–6.0	6.0–4.0	4.0–3.0	3.0–2.5	2.5–2.0	2.0–1.5	1.5–1.41
Unique reflections	301,191	3,848	9,385	18,157	22,826	51,699	145,317	49,959
Completeness (%)	99.1	95.9	99.5	99.1	99.1	99.4	99.6	97.1
$\langle I/\sigma \rangle$	17.2	49.1	51.7	43.5	29.2	23.2	11.0	5.0
Mean redundancy	4.0	6.0	6.8	5.7	3.8	3.7	3.7	3.5
R_{meas} (%) [a]	4.7	3.2	3.5	4.1	4.5	5.4	9.9	25.3
$R_{mrgd\text{-}F}$ (%) [a]	4.6	1.5	1.5	2.0	2.6	3.4	7.4	15.9

[a] R_{meas} and $R_{mrgd\text{-}F}$ as defined by Diederichs and Karplus (1997) are quality measures of the individual intensity observations and of the reduced structure factor amplitudes, respectively.

tional refinement (including noncrystallographic symmetry (NCS) restraints) using data from 100–3.0 Å further reduced the free *R*-factor to 34.6%. The initial $2F_o - F_c$ map displayed well-defined electron density for both dimers in the asymmetric unit. No clear density was seen for residues 5–10, 63–70, 100–120, 170–190, 318–333, and 370–380 (see also Results and discussion). Model building was performed with the program O (Jones et al., 1991). At this stage, four residues were inserted at the N-terminus and deleted from the C-terminus and side chains were changed according to the correct sequence of BB-CK. Several rounds of minimization, simulated annealing (Brünger, 1988), *B*-factor refinement and manual corrections of the model were carried out using data from 6–2.5 Å that lowered R_{free} to 28.4%. The geometry of the model was restrained to the standard parameters of Engh and Huber (1991). At this resolution, residues 2–8, 319–333, and 370–381 could not be modeled into electron density.

In the meantime, low temperature synchrotron data became available (dataset BBCK-2) with a resolution limit of 1.41 Å. Fractionalization followed by re-orthogonalization of the coordinates into the new cell was used to adapt the model to the slightly decreased unit cell volume. All reflections (38–1.41 Å) were used in the refinement procedure and the test set size for cross validation was 5%. Further refinement was performed with the developmental version of CNS (CNS version 0.3–0.5; Brünger et al., 1998), which includes maximum likelihood refinement targets (Pannu & Read, 1996) as well as routines for anisotropic scaling and automatic bulk solvent correction. NCS restraints were completely released in the refinement against high-resolution data. Initial minimization of the slightly distorted model followed by generation of σ_A-weighted $2F_o - F_c$ maps (Read, 1986) of excellent quality now allowed N- and C-termini to be placed unambiguously into electron density. Incorporation of 1,467 water molecules, 1 calcium ion, and 6 acetate molecules into the model was done using X-SOLVATE/X-LIGAND of the program package Quanta97 (MSI, San Diego, California), which utilizes a density peak search algorithm as well as geometric restraints to identify potential solvent or ligand molecules. Waters were only kept if there was at least one potential hydrogen bonding partner and the *B*-factor did not exceed 60 $Å^2$. The calcium ion could easily be identified by its octahedral coordination pattern and smaller interatomic distances. Final free and crystallographic *R*-factors were 22.3 and 20.1%, respectively. The availability of high resolution data gave reason for an additional anisotropic refinement using SHELX-97 (Sheldrick & Schneider, 1997). The model was first subjected to 20 cycles of conventional (isotropic) least-squares refinement using all data. Reflections for the determination of R_{free} were inherited from CNS refinement. R_{free} was 23.4%, which is considerably higher than the value from refinement with CNS, whereas R_{cryst} was 19.5%. This is most likely due to the more sophisticated solvent model and the maximum likelihood target used in CNS. Therefore, only data from 6–1.41 Å were used in subsequent refinement rounds. By changing to individual, restrained anisotropic refinement, R_{free} dropped by 2.6% (R_{cryst} by 3.5%). Finally, 15 disordered residues were included into the model and riding hydrogens were added by SHELX-97. The refinement converged at an R_{free} of 18.8% and R_{cryst} of 13.4%.

In the final model, all residues except those in the highly flexible loop (321–331), which lacks significant density, could be unambiguously modeled into the electron density map. Weak density remained for side chains of the second flexible loop (66–70). Alternative conformations were assigned to residues 38, 48, 88, 137, 236, 240, 252 (Monomer B); 12, 48, 157, 240, 268, 359 (Monomer C); and 12, 38 (Monomer D).

The quality of the final model was assessed with Procheck (Laskowski et al., 1993) and built-in features of CNS and SHELX-97. It has 90.5% of all residues in most favorable, 8.8% in additionally allowed and 0.7% in generously allowed regions of the Ramachandran plot. Three residues (Val325(B), Thr322(C), and Thr327(D)) are in the disallowed region of the Ramachandran plot. They all belong to a flexible loop (321–331), where no significant density could be found. The model exhibits good stereochemistry with standard deviations of 0.011 Å (bonds) and 0.029 Å (angle distances) from standard values (Engh & Huber, 1991).

Coordinates and measured intensities for chicken BB-CK have been deposited in the Brookhaven Protein Data Bank (PDB, accession code 1QH4 and R1QH4SF, respectively).

Acknowledgments

We are very grateful to S. Mühlebach and J.-C. Perriard for providing the chicken B_b-CK cDNA. M. Stolz is acknowledged for cloning of the cDNA into the expression vector and for initial help in protein purification. We thank P. Tucker from EMBL Hamburg for assistance during data collection at beamline BW7B at DESY Hamburg and D.R. Madden for carefully reading the manuscript. This work was supported in part by an ETH graduate training grant for M.E. and by the Swiss National Science Foundation (SNF grant No.3100-5082.97 to T.W. and U.S.).

References

Aksenov MY, Aksenova, MV, Payne RM, Smith CD, Markesbery WR, Carney JM. 1997. The expression of creatine kinase isoenzymes in neocortex of patients with neurodegenerative disorders: Alzheimer's and Pick's disease. *Exp Neurol 146*:458–465.

Bergnes G, Yuan W, Khandekar VS, O'Keefe MM, Martin KJ, Teicher BA, Kaddurah-Daouk R. 1996. Creatine and phosphocreatine analogs: Anticancer activity and enzymatic analysis. *Oncology Research 8*:121–30.

Beuchter DD, Medzihradsky, KF, Burlingame AL, Kenyon GL. 1992. The active site of creatine kinase. Affinity labeling of cysteine 282 with epoxycreatine. *J Biol Chem 267*:2172–2178.

Brünger AT. 1988. Crystallographic refinement by simulated annealing. Application to a 2.8 Å structure of aspartate aminotransferase. *J Mol Biol 203*:803–816.

Brünger AT. 1992a. Free *R* value: A novel statistical quantity for assessing the accuracy of crystal structures. *Nature 355*:472–475.

Brünger AT. 1992b. *X-PLOR version 3.1: A system for X-ray crystallography and NMR.* New Haven, CT: Yale University Press.

Brünger AT, Adams PD, Clore GM, DeLano WL, Gros P, Grosse-Kunstleve RW, Jiang JS, Kuszewski J, Nilges M, Pannu NS, et al. 1998. Crystallography & NMR system (CNS): A new software system for macromolecular structure determination. *Acta Crystallogr D 54*:905–921.

Ch'ng JL, Ibrahim B. 1994. Transcriptional and posttranscriptional mechanisms modulate creatine kinase expression during differentiation of osteoblastic cells. *J Biol Chem 269*:2336–2341.

Chida K, Kasahara K, Tsunenage M, Kohno Y, Yamada S, Ohmi S, Kuroki T. 1990. Purification and identification of creatine phosphokinase B as a substrate of protein kinase C in mouse skin in vivo. *Biochem Biophys Res Commun 173*:351–357.

David S, Shoemaker M, Haley BE. 1998. Abnormal properties of creatine kinase in Alzheimer's disease brain: Correlation of reduced enzyme activity and active site photolabeling with aberrant cytosol-membrane partitioning. *Mol Brain Res 54*:276–287.

Diederichs K, Karplus PA. 1997. Improved R-factors for diffraction data analysis in macromolecular crystallography. *Nature Struct Biol 4*:269–275.

Engh RA, Huber R. 1991. Accurate bond and angle parameters for X-ray protein structure refinement. *Acta Crystallogr A 47*:392–400.

Eppenberger HM, Dawson DM, Kaplan NO. 1967. The comparative enzymology of creatine kinases. Isolation and characterization from chicken and rabbit tissues. *J Biol Chem 242*:204–209.

Forstner M, Kriechbaum M, Laggner P, Wallimann T. 1998. Structural changes of creatine kinase upon substrate binding. *Biophys J 75*(2):1016–1023.

Forstner M, Müller A, Stolz M, Wallimann T. 1997. The active site histidines of creatine kinase. A critical role of His61 situated on a flexible loop. *Protein Sci 6*:331–339.

Friedman DL, Roberts R. 1992. Purification and localization of brain-type creatine kinase in sodium chloride transporting epithelia of the spiny dogfish, *Squalus acanthias*. *J Biol Chem 267*:4270–4276.

Fritz-Wolf K, Schnyder T, Wallimann T, Kabsch W. 1996. Structure of mitochondrial creatine kinase. *Nature 381*:341–345.

Furter R, Furter-Graves EM, Wallimann T. 1993. The reactive cysteine is required for synergism but is nonessential for catalysis. *Biochemistry 32*:7022–7029.

Furter R, Kaldis P, Furter-Graves EM, Schnyder T, Eppenberger HM, Wallimann T. 1992. Expression of active octameric cardiac mitochondrial creatine kinase in *Escherichia coli*. *Biochem J 288*:771–775.

Gross M, Lustig A, Wallimann T, Furter R. 1995. Multiple-state equilibrium unfolding of guanidino kinases. *Biochemistry 34*:10350–10357.

Grossman SH. 1990. Resonance energy transfer between the active site of rabbit muscle creatine kinase by steady-state and time-resolved fluorescence. *Biochemistry 28*:4894–4902.

Guerrero LM, Beron J, Spindler B, Groscurth P, Wallimann T, Verrey F. 1997. Metabolic support of Na^+-pump in apically permeabilized A6 kidney cell epithelia: Role of creatine kinase. *Am J Physiol 272*:C697–C706.

Hemmer W, Furter-Graves EM, Frank G, Wallimann T, Furter R. 1995. Autophosphorylation of creatine kinase: Characterization and identification of a specifically phosphorylated peptide. *Biochim Biophys Acta 1251*:81–90.

Hossle JP, Rosenberg UB, Schafer HM, Eppenberger HM, Perriard J-C. 1986. The primary structure of chicken creatine kinase and evidence for heterogeneity of its mRNA. *Nucl Acids Res 14*:1449–1463.

Hou ZX, Vollmer S. 1994. The activity of S-thiomethyl modified creatine kinase is due to regeneration of free thiol at the active site. *Biochim Biophys Acta 1205*:83–88.

Jones TA, Zou J-Y, Cowan SW, Kjeldgaard M. 1991. Improved methods of building protein models in electron density maps and the location of errors in these models. *Acta Crystallogr A 47*:110–119.

Kabsch W. 1988. Evaluation of single-crystal X-ray diffraction data from a position-sensitive detector. *J Appl Crystallogr 21*:916–924.

Kabsch W. 1993. Automatic processing of rotation diffraction data from crystals of initially unknown symmetry and cell constants. *J Appl Crystallogr 26*:795–800.

Kabsch W, Fritz-Wolf K. 1997. Mitochondrial creatine kinase—A square protein. *Curr Opin Struct Biol 7*:811–818.

Kabsch W, Sander C. 1983. Dictionary of protein secondary structure: Pattern recognition of hydrogen-bonded and geometrical features. *Biopolymers 22*:2577–2637.

Kaddurah-Daouk R, Lillie JW, Daouk GH, Green MR, Kingston R, Schimmel P. 1990. Induction of a cellular enzyme for energy metabolism by transforming domains of adenovirus E1a. *Mol Cell Biol 10*:1476–1483.

Kaldis P, Furter R, Wallimann T. 1994. The N-terminal heptapeptide of mitochondrial creatine kinase is important for octamerization. *Biochemistry 33*:952–959.

Kaldis P, Hemmer W, Zanolla E, Holtzman D, Wallimann T. 1996. Hot spots of creatine kinase localization in brain: Cerebellum, hippocampus and choroid plexus. *Dev Neurosci 18*:542–554.

Kraulis PJ. 1991. MOLSCRIPT: A program to produce both detailed and schematic plots of protein structures. *J Appl Crystallogr 24*:946–950.

Kültz D, Somero GN. 1995. Ion transport in gills of the euryhaline fish *Gillichtys mirabilis* is facilitated by a phosphocreatine circuit. *Am J Physiol 268*:R1003–R1012.

Larsen TA, Olson AJ, Goodsell DS. 1998. Morphology of protein-protein interfaces. *Structure 6*:421–427.

Laskowski RA, MacArthur MW, Moss DS, Thornton JM. 1993. PROCHECK: A program to check the stereochemical quality of protein structures. *J Appl Crystallogr 26*:283–291.

Liaw SH, Jun G, Eisenberg D. 1994. Interactions of nucleotides with fully unadenylylated glutamine synthetase from *Salmonella typhimurium*. *Biochemistry 33*:11184–11188.

Luzatti V. 1952. Traitement statistique des erreurs dans la determination des structures cristallines. *Acta Crystallogr 5*:802–810.

Marcillat O, Goldschmidt D, Eichenberger D, Vial C. 1987. Only one of the two interconvertible forms of mitochondrial creatine kinase binds to heart mitoplasts. *Biochim Biophys Acta 890*:233–241.

McRee DE. 1992. A visual protein crystallographic software system for X11/Xview. *J Mol Graph 10*:44–46.

Merritt EA, Bacon DJ. 1997. Raster3D: Photorealistic molecular graphics. *Methods Enzymol 277*:505–524.

Milner-White EJ, Watts DC. 1971. Inhibition of adenosine 5′-triphosphate-creatine phosphotransferase by substrate-anion complexes. Evidence for the transition-state organization of the catalytic site. *Biochem J 122*(5):727–740.

Min KL, Steghens JP, Henry R, Doutheau A, Collombel C. 1998. Identification of the creatine binding domain of creatine kinase by photoaffinity labeling. *Biochim Biophys Acta 1387*:80–88.

Mühlebach SM, Gross M, Wirz T, Wallimann T, Perriard J-C, Wyss M. 1994. Sequence homology and structure predictions of the creatine kinase isoenzymes. *Mol Cell Biochem 133/134*:245–262.

Navaza J. 1994. AmoRe: An automated package for molecular replacement. *Acta Crystallogr D 50*:157–163.

Pannu NS, Read RJ. 1996. Improved structure refinement through maximum likelihood. *Acta Crystallogr A 52*:659–668.

Payne MR, Friedman DL, Grant JW, Perryman MB, Strauss AW. 1993. Creatine kinase isoenzymes are highly regulated during pregnancy in rat uterus and placenta. *Am J Physiol 265*:E624–E635.

Quest AFG, Soldati T, Hemmer W, Perriard J-C, Eppenberger HM, Wallimann T. 1990. Phosphorylation of chicken brain-type creatine kinase affects a physiologically important kinetic parameter and gives rise to protein microheterogeneity in vivo. *FEBS 2*:457–464.

Raimbault C, Buchet R, Vial C. 1996. Changes of creatine kinase secondary structure induced by the release of nucleotides from caged compounds. *Eur J Biochem 240*:134–142.

Rao JK, Bujacz G, Wlodawer A. 1998. Crystal structure of rabbit muscle creatine kinase. *FEBS 439*:133–137.

Read RJ. 1986. Improved Fourier coefficients for maps using phases from partial structures with errors. *Acta Crystallogr A 42*:140–149.

Reiss NA, Kaye A. 1981. Identification of the major component of the estrogen-induced protein of rat uterus as the BB isoenzyme of creatine kinase. *J Biol Chem 256*:5741–5749.

Ritchie M-E, Trask RV, Fontanet HL, Billadello JJ. 1991. Multiple positive and negative elements regulate human brain creatine kinase gene expression. *Nucl Acids Res 19*:6231–6240.

Rojo M, Hovius R, Demel R, Wallimann T, Eppenberger HM, Nicolay K. 1991. Interaction of mitochondrial creatine kinase with model membranes. A monolayer study. *FEBS 1,2*:123–129.

Rossmann MG. 1972. *The molecular replacement method*. New York: Gordon and Breach.

Samuels AJ. 1961. Immunoenzymological evidence suggesting a change in conformation of adenylic acid deaminase and creatine kinase during substrate combination. *Biochem J 1*:437–444.

Schlattner U, Forstner M, Eder M, Stachowiak O, Fritz-Wolf K, Wallimann T. 1998. Functional aspects of the X-ray structure of mitochondrial creatine kinase: A molecular physiology approach. *Mol Cell Biochem 184*:125–140.

Schlegel J, Wyss M, Schürch U, Schnyder T, Quest A, Wegmann G, Eppenberger HM, Wallimann T. 1988a. Mitochondrial creatine kinase from cardiac muscle and brain are two distinct isoenzymes but both form octameric molecules. *J Biol Chem 263*:16963–16969.

Schlegel J, Zurbriggen B, Wegmann G, Wyss M, Eppenberger HM, Wallimann T. 1988b. Native mitochondrial creatine kinase (Mi-CK) forms octameric structures. I. Isolation of two interconvertible Mi-CK isoforms: Dimeric and octameric Mi-CK. *J Biol Chem 263*:16942–16953.

Shatton JB, Morris HP, Weinhouse S. 1979. Creatine kinase activity and isoenzyme composition in normal tissue and neoplasms of rat and mice. *Cancer Res 39*:492–501.

Sheldrick GM, Schneider TR. 1997. SHELXL: High resolution refinement. *Methods Enzymol 277*:319–343.

Sistermans EA, Klaassen CHW, Peters W, Swarts HGP, Jap PHK, DePont JJHHM, Wieringa D. 1995. Co-localization and functional coupling of creatine kinase B and gastric H^+/K^+-ATPase on the apical membrane and the tubovesicular system of parietal cells. *Biochem J 311*:445–451.

Soldati T, Schäfer B, Perriard J-C. 1990. Alternative ribosomal initiation gives rise to chicken brain-type creatine kinase isoproteins with heterogeneous amino termini. *J Biol Chem 265*:4498–4506.

Sömjen D, Weisman Y, Harell A, Berger E, Kaye AM. 1989. Direct and sex-specific stimulation by sex steroids of creatine kinase activity and DNA synthesis in rat bone. *Proc Natl Acad Sci USA 86*:3361–3365.

Stolz M, Wallimann T. 1998. Myofibrillar interaction of cytosolic creatine kinase (CK) isoenzymes: Allocation of N-terminal binding epitope in MM-CK and BB-CK. *J Cell Sci 111*:1207–1216.

Stroud RM. 1996. Balancing ATP in the cell. *Nature Struct Biol 3*:567–569.

Suzuki T, Kawasaki Y, Furukohri T, Ellington WR. 1997. Evolution of phosphagen kinase. VI. Isolation, characterization and cDNA-derived amino acid sequence of lombricine kinase from the earthworm *Eisenia foetida*, and identification of a possible candidate for the guanidine substrate recognition site. *Biochim Biophys Acta 1348*:152–159.

Ventura-Clapier R, Veksler V, Hoerter JA. 1994. Myofibrillar creatine kinase and cardiac contraction. *Mol Cell Biochem 133/134*:125–144.

Wallimann T, Hemmer W. 1994. Creatine kinase in non-muscle tissues and cells. *Mol Cell Biochem 133/134*:193–220.

Wallimann T, Moser H, Eppenberger HM. 1983. Isoenzyme-specific localization of M-line bound creatine kinase in myogenic cells. *J Muscle Res Cell Motil 4*:429–441.

Wallimann T, Wyss M, Brdicka D, Nicolay K, Eppenberger HM. 1992. Intracellular compartmentation, structure and function of creatine kinase isoenzymes in tissues with high and fluctuating energy demands: The "phosphocreatine circuit" for cellular energy homeostasis. *Biochem J 281*: 21–40.

Wirz T, Brandle U, Soldati T, Hossle JP, Perriard J-C. 1990. A unique chicken B-creatine kinase gene gives rise to two B-creatine kinase isoproteins with distinct N-termini by alternative splicing. *J Biol Chem 265*:11656–11666.

Xu CJ, Klunk WE, Kanfer JN, Xiong Q, Miller G, Pettegrew JW. 1996. Phosphocreatine-dependent glutamate uptake by synaptic vesicles. A comparison with ATP-dependent glutamate uptake. *J Biol Chem 271*:13435–13440.

Zhao J, Schmieg FI, Simmons DT, Molloy GR. 1994. Mouse p53 represses the rat brain creatine kinase gene but activates the rat muscle creatine kinase gene. *Mol Cell Biol 14*:8483–8492.

Zhou G, Somasundaram T, Blanc E, Parthasarathy G, Ellington WR, Chapman MS. 1998. Transition state structure of arginine kinase: Implications for catalysis of bimolecular reactions. *Proc Natl Acad Sci USA 95*:8449–8454.